Dalton Transactions

Accepted Manuscript

ROYAL SOCIETY OF CHEMISTRY

www.rsc.org/dalton

Table of contents

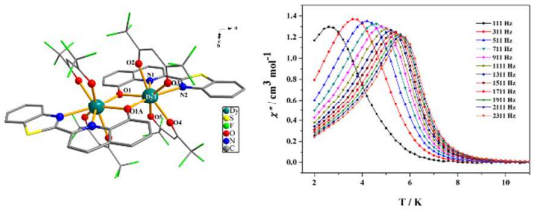

New lanthanide complexes based on tridentate ligand derived from 8-hydroxyquinoline were synthesized. Luminescence properties and single-molecule magnet behavior were investigated.

Luminescence, magnetocaloric effect and single-molecule magnet behavior in lanthanide complexes based on tridentate ligand derived from 8-hydroxyquinoline

Hai-Yun Shen, [a] Wen-Min Wang, [a] Yan-Xia Bi, [a] Hong-Ling Gao, [a] Shuang Liu, [b] Jian-Zhong Cui *[a]

Abstract

A new family of lanthanide complexes, $[Ln_2(hfac)_4L_2]$ (Ln = Eu (**1**), Gd (**2**), Tb (**3**), Dy (**4**), Ho (**5**), Er (**6**), Lu (**7**); hfac = hexafluoroacetylacetonate, HL = 2-(2′-benzothiazole)-8-hydroxyquinoline), was synthesized and characterized using single-crystal X-ray diffraction, elemental analysis (EA), thermal gravimetric analysis (TGA), powder X-ray diffraction (PXRD) and UV-vis spectra. X-ray crystallographic analyses reveal that **1**–**7** are isomorphous and crystallize in the monoclinic space group *C2/c*. In these dinuclear complexes, each Ln^{III} ion is eight-coordinated with two bidentate hfac and two μ-phenol bridging L ligands. The TGA results show that the complexes have relatively high thermal stabilities. Complexes **1** and **3** show the characteristic transitions of corresponding lanthanide ions with ligand-related emission peaks. Meanwhile, complexes **4** and **7** exhibit ligand-centered fluorescence at room temperature. Magnetic measurements were carried out on complexes **2**–**6**. The magnetic study reveals that **2** displays a magnetocaloric effect, with a maximum $-\Delta S_m$ value of 16.89 J K^{-1} kg^{-1} at 2 K for ΔH = 8 T. Dynamic magnetic studies reveal single-molecule magnet (SMM) behavior for complex **4.** Fitting the dynamic magnetic data to the Arrhenius law gives an energy barrier $\Delta E/k_B$ = 50.33 K and pre-exponential factor $\tau_0 = 1.05\times10^{-8}$ s.

[a] *Department of Chemistry, Tianjin University, Tianjin 300072, P. R. China.*
E-mail: cuijianzhong@tju.edu.cn
[b] *School of Chemistry and Chemical Engineering, Xi'an Shiyou University, Xi'an, Shaanxi Province,710065, P. R. China*.
Electronic supplementary information (ESI) available: Supplementary Experimental Section. Tables of selected bond lengths and angles. Fig. S1 to S10. CCDC: 1413617(**1**), 1404077-1404081(**2**–**6**) and 1413618(**7**).

Introduction

Lanthanide ions are commonly employed in modern technologies because of their intrinsic luminescence and magnetic properties. For photoluminescence, lanthanide ions can show characteristic narrow line-like emissions of pure colors,[1] due to the shielding of the 4f orbits by the full $5p^6 6s^2$ subshells. Meanwhile, lanthanide ions have other unique features, such as high luminescence quantum yield, long-lived emission, and large Stokes shifts.[2] These properties make them potential candidates for fluorescent probes, light-emitting diodes, and the conversion or amplification of light.[3] The photoluminescence properties of Ln^{III} complexes have been widely investigated. Especially, Eu^{III} and Tb^{III} complexes have been drawing significant interest due to their strong, easily detected emissions in the visible region, while Nd^{III}, Er^{III} and Yb^{III} complexes have been widely noted and studied in the near-infrared (NIR) regions.[4] For magnetic properties, because of the different local magnetic anisotropy and the large-spin multiplicity of the spin ground-state, 4f lanthanide elements, have been widely used to construct molecule-based magnetic materials. These molecule-based magnetic materials, have huge potential applications, including high-density information storage,[5] quantum computing,[6] molecule-based spintronics devices[7] and magnetic refrigeration.[8] Furthermore, such molecule-based magnetic materials permit the observation of fascinating physical phenomenon such as quantum tunneling of magnetization,[9] quantum coherence,[10] quantum super position,[11] magnetic deflagration,[12] and so on. The design of molecule-based magnetic materials, has attracted extensive interest during the past decade, especially Dy^{III} complexes for single molecule magnets (SMMs)[13] and Gd^{III} complexes for low-temperature molecular magnetic coolers (MMCs).[14]

So far, there has been very limited work on the magnetic properties of lanthanide

complexes based on 8-hydroxyquinoline and its derivatives, and to the best of our knowledge, there are only a few reports of SMMs among them.[15] Accordingly, we assembled 2-(2′-benzothiazole)-8-hydroxyquinoline (HL) in this report. The ligand has attracted attention because it can advantageously combine a monoanionic rigid tridentate N, N, O-chelating unit for metal binding. Moreover, the phenol atom of HL can be deprotonated to act as a bridge between lanthanide centers, which contributes to efficient magnetic exchange between neighboring magnetic carriers. Taking advantage of the strong electron-withdrawing effect of hexafluoroacetylacetonate, we report herein the successful assembly of seven dinuclear lanthanide complexes $[Ln_2(hfac)_4L_2]$ (Ln = Eu (**1**), Gd (**2**), Tb (**3**), Dy (**4**), Ho (**5**), Er (**6**), Lu (**7**)). Magnetic measurements on complexes **2**–**6** were carried out. Magnetic studies reveal single-molecule magnet (SMM) behavior for complex **4**; meanwhile, complex **2** displays a magnetocaloric effect. The luminescence properties of **1**, **3**, **4**, **6** and **7** were also investigated.

Results and discussion

Crystal structure descriptions.

X-ray crystallographic analyses reveal that **1**–**7** are isomorphic dinuclear complexes and crystallize in the monoclinic *C2/c* space group. Therefore, as a representative, only the structure of complex **1** is discussed in detail (Fig. 1a). The Eu^{III} ions are eight-coordinated by four oxygen atoms from two hfac anions, two oxygen atoms from the μ-phenol of the L ligands, two nitrogen atoms from the quinoline ring and benzothiazole ring. The lengths of the Eu–O bonds are in the range of 2.336(2)–2.414(2) Å and the Eu–N bond distances are 2.492(3) and 2.608(3) Å for complex **1**. Two Eu^{III} ions are bridged by the μ-phenol atoms from two ligands (L), with Eu–O bond lengths of 2.396(2) and 2.336(2) Å, an Eu···Eu distance of 3.8195(8) Å, and an Eu–O–Eu angle of 107.64 (8)°. The quinoline and benzothiazole rings in the two L ligands are nearly coplanar. Here, the eight-coordinated Eu1

center demonstrates a distorted dodecahedron geometry (Fig. 1b). Selected bond lengths and angles for complexes **1–7** are listed in Tables S1–S7 in the electronic supplementary information (ESI).

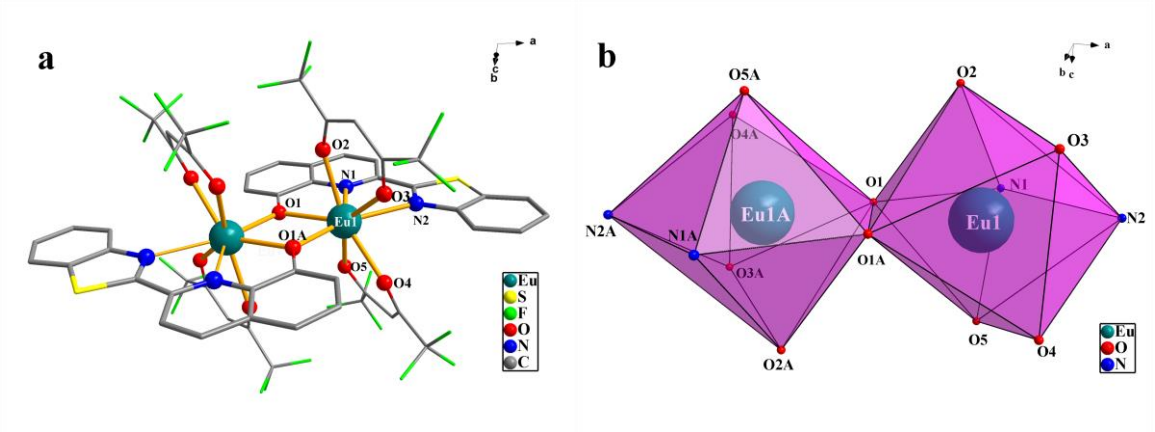

Fig. 1 (a) Molecular structure of complex **1**. Hydrogen atoms have been omitted for clarity. **(b)** The coordination geometries for the Eu1 and Eu1A atoms in complex **1**. Symmetry code: #1 -x+1/2, -y+1/2, -z.

Thermal gravimetric analysis and powder X-ray diffraction.

To investigate the thermal stabilities of these complexes, thermal gravimetric analyses of complexes **1–7** were performed under air atmosphere in the temperature range of 30 to 800 °C. TGA curves of **1**–**7** (Fig. S1, ESI) have similar profiles, exhibiting two main weight loss steps until the decomposition of the framework. Therefore, as a representative, only the TGA curve of **1** is discussed in detail. The TGA curve of **1** indicates thermal stability up to 340 °C, and then the weight loss of 49.61% in the range of 340 to 390 °C is attributed to the loss of four coordinated hfac ligands, which is consistent with the calculated value (49.10%). After that the framework decomposes gradually. Finally, the residue of 21.68% (calcd. 20.86%) is expected to be the corresponding lanthanide oxide Eu_2O_3. The TGA results show that the thermal decomposition temperatures of the complexes are very high. The good thermal stabilities of the complexes may exist due to the fact that the M-O bonds are highly polarized.[16]

The crystalline products of **1**–**7** were characterized using X-ray powder diffraction

(PXRD) at room temperature (Fig. S2, ESI). These results are in good agreement with the XRD patterns simulated from the single-crystal data, indicating high purity of the obtained samples. The differences in intensity may be due to the preferred orientations of the crystalline powder samples.

UV-vis spectra.

The UV-vis absorption spectra of $Eu(hfac)_3 \cdot 2H_2O$, the ligand and their complexes **1**–**7**, recorded in CH_2Cl_2 solution at 10^{-5} mol/L and room temperature, are depicted in Fig. 2. $Eu(hfac)_3 \cdot (H_2O)_2$ has one absorption band centered ca. 300 nm and almost no absorption above 350 nm. The absorption spectum of the ligand has three bands in the spectral range of 250–400 nm; the lowest energy transition is observed at 340–358 nm with an absorption cutoff at 400 nm due to $\pi \rightarrow \pi^*$ transitions within the quinoline and benzothiazole chromophores. Upon deprotonation and complex formation, the absorption band at 340–358 nm is red-shifted to 352–370 nm. In the UV-vis spectra of **1**–**7**, there are three sets of absorption bands: one from the intraligand π-π* transition of hfac and ligand ca. 300 nm and the other ca. 352–370 nm from the intraligand π-π* transition. In addition, a broad low-energy absorption band appears in the visible range with a maximum at 500 nm. $Ln(hfac)_3 \cdot (H_2O)_2$ and the ligand have almost no absorption above 400 nm, while **1**–**7** exhibit appreciable absorption bands in the region of 400–500 nm, most likely arising from an intraligand phenolate-to-pyridyl charge transfer (ILCT) within the 8-hydroxyquinolate chromophore.[17]

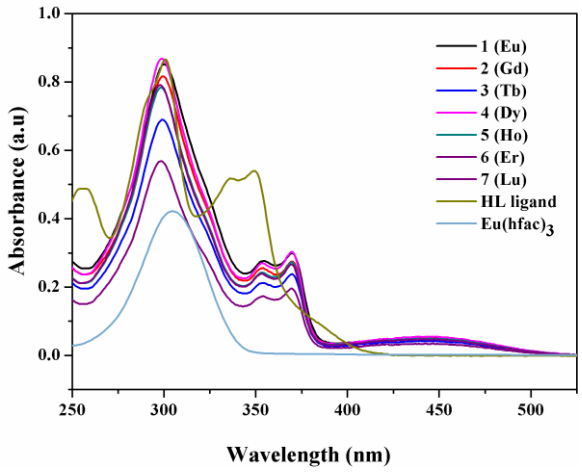

Fig. 2 UV-vis absorption spectra of complexes **1**–**7** in CH_2Cl_2 solution at room temperature.

Luminescence properties.

The luminescent properties of the ligand and lanthanide complexes **1**, **3**, **4** and **7** in methanol solution at 10^{-5} mol/L were investigated at room temperature. The excitation spectra of **1**, **3** and **4** were recorded by monitoring at 617 nm for **1**, 545 nm for **3** and 575 nm for **4** (Fig. S3, ESI). The spectra of **1** and **3** display broad bands centered at 294 nm, while the excitation spectrum of **4** shows a broad band centered at 275 nm, which can be attributed to intraligand charge transfer (ILCT).

As shown in Fig. 3a, the emission spectrum of **1** exhibits the typical emission bands of the Eu^{III} ion centered at 589, 617, 653 and 694 nm, which are assigned to the transitions of $^5D_0$ to ^7F_J (J = 1, 2, 3, 4).[18] The intensity of the electric dipole-allowed $^5D_0 \rightarrow {}^7F_2$ transition (617 nm) was much stronger than that of the magnetic dipole-allowed $^5D_0 \rightarrow {}^7F_1$ transition (589 nm), indicating that the Eu^{III} ion in the complex occupied a very low symmetry site. In addition to the Eu^{III} ion peaks, a broad emission band centered at 350 nm is also detected, which results from the ligand fluorescence and indicates that efficiency of energy transfer from the ligands to the ions is not ideal. The commonly accepted energy transfer pathway for the sensitization of Ln^{III} ion luminescence consists of excitation of the ligand into its excited singlet states, subsequent intersystem crossing to triplet states, and then energy transfer from the lowest

triplet level to an excited state of the lanthanide ion through a nonradiative transition.[19] To make energy transfer effective, the triplet states of the ligand and the accepting lanthanide energy level should be matched. According to Latva's empirical rule,[20] an optimal ligand-to-metal energy transfer process for Eu^{III} needs an energy gap ΔE ($^3\pi\pi^*-5D_0$) > 2500 cm^{-1}. The lowest excited energy level of the Eu^{III} ion is located at 17500 cm^{-1}($^5D_0$, 570 nm), which means the triplet states of the ligand should be at least higher than 20000 cm^{-1}(500 nm). However, 8-hydroxyquinoline and its derivatives have low energy triplet states at approximately 17100 cm^{-1} (585 nm).[21] This feature is the reason that energy can not transfer from the L ligand to the Eu^{III} ions. The triplet energy level of the hexafluoroacetylacetone ligand (22200 cm^{-1}) lies above the resonant level of Eu^{III} (17500 cm^{-1}, $^5D_0$), allowing an efficient ligand-to-metal energy transfer. Thus, the emission spectrum of **1** exhibits the typical emission bands of the Eu^{III} ion due to the chelating hfac ligand.

For complex **3**, the emission spectrum is shown in Fig. 3b, where f – f transitions of the Tb^{III} ion with ligand-centered emission are observed. Upon excitation at 294 nm, three characteristic weak luminescent bands from Tb^{III} appear. The first emission band at 491 nm can be assigned to $^5D_4 \rightarrow {}^7F_6$ transitions, while the other bands at 545, 585 and 626 nm can be attributed to the $^5D_4 \rightarrow {}^7F_5$, $^5D_4 \rightarrow {}^7F_4$ and $^5D_4 \rightarrow {}^7F_3$ transitions,[22] respectively. Ligand-centered emission is observed due to the energy level mismatch between the L ligand and the lanthanide, while the typical emission bands of the Tb^{III} ion appear due to the higher triplet energy level of the hfac ligand compared with the lowest excited level of Tb^{III} (20500 cm^{-1}, $^5D_4$), allowing an efficient ligand-to-metal energy transfer.

Different from those of **1** and **3**, no characteristic peaks of Dy^{III} ion are observed in the spectrum of Dy^{III} complex (Fig. S4, ESI) at room temperature except for broad emission bands at 326 and 630 nm, originating from an intraligand $\pi \rightarrow \pi^*$ transition of ligands. This is mostly because of close energy gap of the triplet state in the hfac ligand and Dy^{III} ($^4F_{9/2}$ =

21100 cm^{-1}, ΔE = 1100 cm^{-1}) resulting in poor energy transfer from the hfac ligands to the Dy^{III} ion.

For complex **7**, the fluorescent spectrum is similar to that of the ligand (Fig. S5, ESI), which originates from ligand centered fluorescence. Because the Lu^{III} ion has a filled 4f shell, no f–f transitions occur and consequently, no emissions in the visible range are observed. However, when the Lu^{III} ion coordinates with an organic ligand to form a metal-organic complex, it can sensitize and enhance the emission of the organic chromophores, perhaps as a result of the metal-ligand coordination, which effectively increases the rigidity of the ligand and reduces the nonradiative decay of the intraligand excited state.[23]

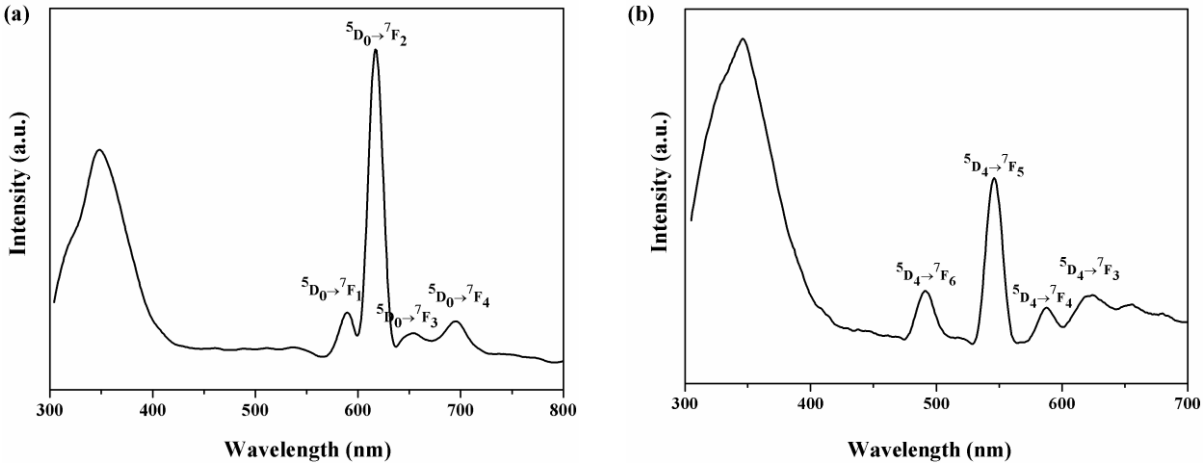

Fig. 3 Room-temperature luminescence spectra of **1** (a) and **3** (b) (λ_{ex} = 294 nm) in the methanol.

Near-infrared luminescent properties.

The luminescence spectrum of complex **6** in the solid-state was investigated upon excitation at 310 nm, displaying typical emissions in the NIR region. The emission spectrum shows a peak at 1533 nm (Fig. S6, ESI), which covers a large spectral range from 1460 to 1633 nm and is attributed to the typical $^4I_{13/2} \rightarrow {}^4I_{15/2}$ transition of Er^{III}.[24] The Er^{III} complexes are particularly interesting for application in amplification because the transition around 1534 nm is in the right position for the third telecommunication window.[25] The triplet energy levels of the hfac and L ligands lie above the emitting level ($^4I_{13/2}$) of Er^{III}, therefore, both ligands are suitable for an effective energy transfer to the Er^{III} ion.

Magnetic properties.

Static magnetic properties. The magnetic susceptibilities of complexes **2**–**6** were measured on powder samples in an applied magnetic field of 1000 Oe over the temperature range 2–300 K. The $\chi_M T$ vs T (χ_M being the molar magnetic susceptibility) and χ_M^{-1} vs T are shown in Fig. 4 and Fig. S8 (ESI).

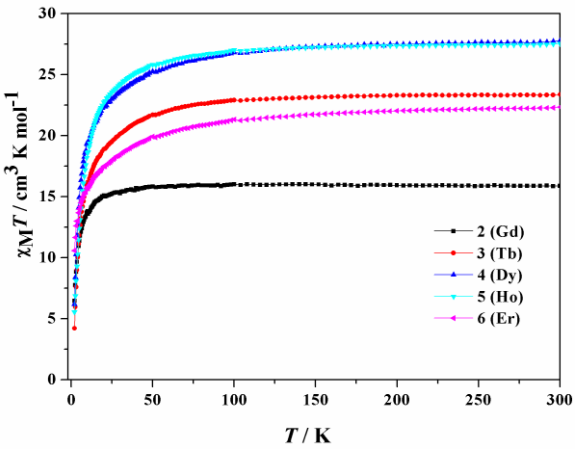

Fig. 4 Temperature dependence of the $\chi_M T$ products in 1000 Oe for complexes **2–6**

For **2**, the $\chi_M T$ value is 15.87 cm^3 K mol^{-1} at 300 K, which is consistent with the expected value of two free Gd^{III} ions (15.76 cm^3 K mol^{-1}, $^8S_{7/2}$, g = 2).[26] As the temperature decreases, the $\chi_M T$ value decreases slowly and almost remains constant until ca. 50 K. On further cooling, the $\chi_M T$ value abruptly decreases to 12.92 cm^3 K mol^{-1} at 2 K. This behavior corresponds to the existence of weak antiferromagnetic interactions between the Gd^{III} ions. Between 2 and 300 K, the linear fit of χ_M^{-1} vs T obeys the Curie-Weiss law, with C = 15.99 cm^3 K mol^{-1} and θ = –1.13 K; the negative θ value also indicates antiferromagnetic interactions between adjacent Gd^{III} ions. As the dinuclear units in complex **2** are well separated from each other, the antiferromagnetic coupling observed most likely originates from intramolecular, the exchange pathway being provided by the double μ-phenol bridges. Consequently, the magnetic data was analyzed by means of a simple dimer law for two interacting spin octets derived through the isotropic spin Hamiltonian $\hat{H} = -J\hat{S}_1 \cdot \hat{S}_2$ (where J

is the exchange coupling parameter, $\hat{S}_1$ and $\hat{S}_2$ are the spin operators of the local spins ($\hat{S}_1 = \hat{S}_2 = 7/2$)). The best-fit parameters obtained from Van Vleck's equation are: J = –0.071 cm^{-1}, g = 2.02 and R = 2.25×10^{-6} (R is the agreement factor defined as $\sum_i\left[(\chi_M T)_{obs}(i)-(\chi_M T)_{cacl}(i)\right]^2 / \sum_i\left[(\chi_M T)_{obs}(i)\right]^2$). The calculated curve matches well the magnetic data in the whole temperature range investigated (Fig. S7, ESI).

In the cases of **3–6**, the $\chi_M T$ values at 300 K are 23.36 cm^3 K mol^{-1} (**3**), 27.77 cm^3 K mol^{-1} (**4**), 27.53 cm^3 K mol^{-1} (**5**) and 22.33 cm^3 K mol^{-1} (**6**). The theoretical values for two isolated Ln^{III} cations follow: two Tb^{III} ($^7F_6$, g = $^3/_2$) are 23.64 cm^3 K mol^{-1} for **3**; two Dy^{III} ($^6H_{15/2}$, g = $^4/_3$) are 28.34 cm^3 K mol^{-1} for **4**; two Ho^{III} ($^5I_8$, g = $^5/_4$) are 28.14 cm^3 K mol^{-1} for **5**; and two Er^{III} ($^4I_{15/2}$, g = $^6/_5$) are 22.96 cm^3 K mol^{-1} for **6**.[26]

For **3–6**, during the cooling process, the $\chi_M T$ values experience almost no change over the temperature range of 300–100 K, which indicates competitive balance between ferromagnetic interactions and thermal depopulation of the Stark sublevels,[27] and then further decrease sharply to reach minima of 4.21 (**3**), 6.19 (**4**), 5.56 (**5**) and 10.58 (**6**) cm^3 K mol^{-1} at 2 K.

In addition, the magnetic susceptibilities of complexes **3–6** can be fitted to the Curie−Weiss law between 2 and 300 K (Fig. S8, ESI), with C = 23.81 cm^3 K mol^{-1}, θ = –5.00K (**3**), C = 28.19 cm^3 K mol^{-1}, θ = –5.37 (**4**), C = 28.00 cm^3 K mol^{-1}, θ = –4.82 K (**5**), C = 22.64 cm^3 K mol^{-1}, θ = –5.79 K (**6**). Due to the larger spin-orbit coupling and magnetic anisotropy of such systems, it is difficult to decide if the negative Weiss temperature indicates antiferromagnetic interactions between adjacent Ln^{III} ions in these complexes.

The magnetization data of **2** were collected at fields of 0–8 T between 2 and 10 K (Fig. 5a), exhibiting a steady increase with increasing H and the saturation values of 13.78 Nβ for **2** at 8 T and 2 K closely approximate the theoretical value of 14 Nβ for two individual Gd^{III}

(S = 7/2, g = 2) ions. The magnetic entropy changes ΔS_m of **2** are calculated by applying the Maxwell equation (ΔS_m (T) = $\int$ [$\partial M(T, H)/\partial T]_H dH$) to obtain the isothermal magnetic entropy changes $-\Delta S_m$ from the experimental magnetization data.[28] For **2**, the changes of magnetic entropy give a maximum value of 16.89 J K^{-1} kg^{-1} (32.63 mJ cm^{-3} K^{-1}) at 2 K for ΔH = 8 T. The expected maximum $-\Delta S_m$ value is 20.37 J K^{-1} kg^{-1}, which was calculated from the equation $-\Delta S_m = N_{Gd} R\ln(2S_{Gd} + 1)$, where N_{Gd} is the number of Gd^{III} present per mole of **2**. The difference in the theoretical and experimental values of $-\Delta S_m$ for **2** may be ascribed to the presence of an antiferromagnetic exchange among the Gd^{III} ions.[29]

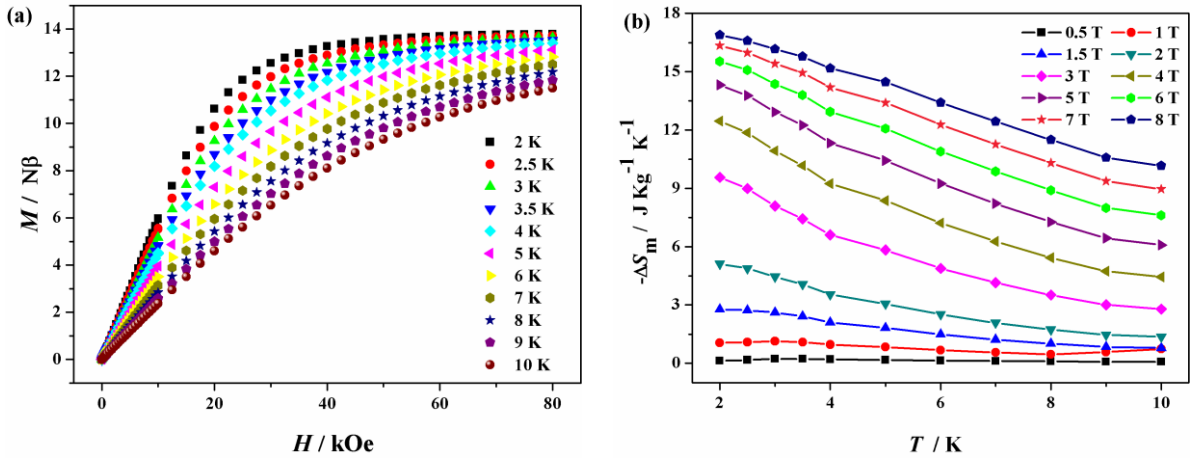

Fig. 5 (a) Magnetization vs applied field of **2** at T = 2.0−10.0 K and H = 0−8 T. (b) ΔS_m calculated using the magnetization data of **2** at different fields and temperatures.

The M vs H/T data for complex **4** measured in different magnetic fields (Fig. S9, ESI) show nonsuperposition, suggesting the presence of magnetic anisotropy and/or low-lying excited states. The maximum magnetization at 2 K and 7 K at 8 T are 14.14 μ_B and 17.30 μ_B, which are lower than the expected saturation value of 20 μ_B for two Dy^{III} ions (10 μ_B for each Dy^{III} ion), most likely because of the crystal field effect in the Dy^{III} ion, which eliminates the 16-fold degeneracy of the $^6H_{15/2}$ ground state.[30]

Dynamic magnetic properties for **4**. To examine the dynamics of the magnetization of **4**,

the temperature and frequency dependencies of the alternating-current (ac) susceptibility were measured under zero dc field in an oscillating ac field of 3 Oe. Both in-phase (χ') and out-of-phase (χ'') susceptibilities show clear frequency and temperature dependences, which both reveal the typical features associated with SMM behavior.

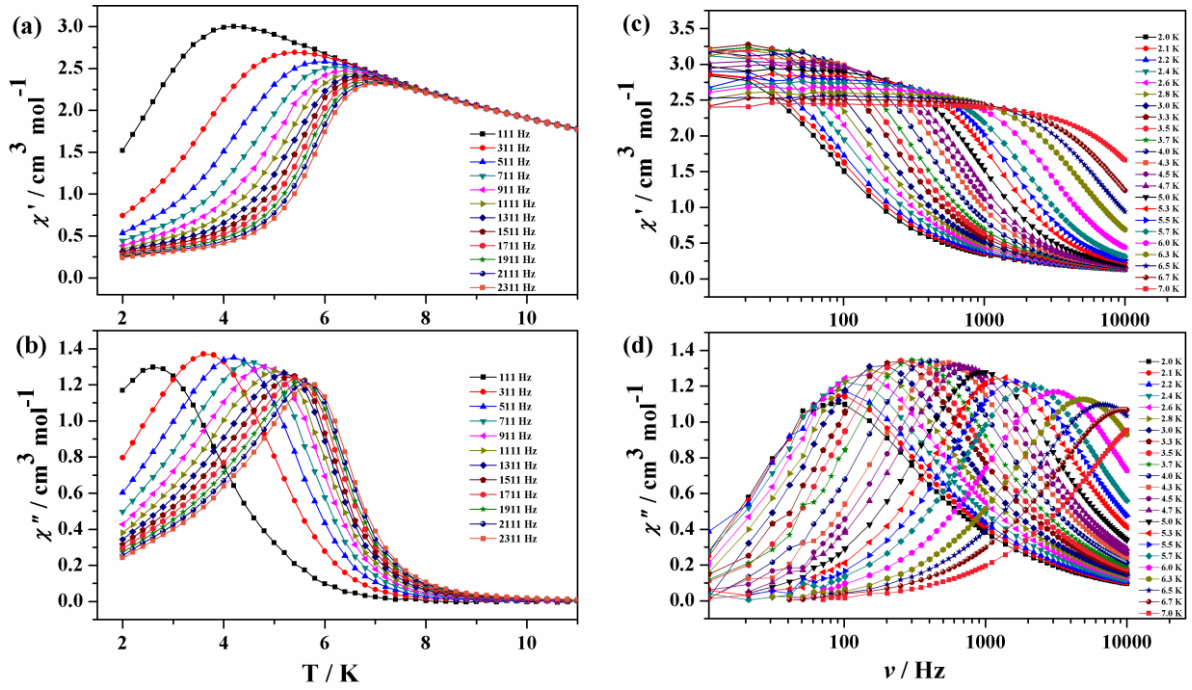

Fig. 6 Temperature dependence (a, b) and frequency dependence (c, d) of *ac* susceptibilities for complex **4** in the absence of *dc* field (*Hac* = 3Oe).

Using the frequency dependencies of the ac susceptibility (Fig. 6d), the magnetization relaxation times (τ) were estimated between 2 and 7 K (Fig. 7). The relaxation energy barrier can be obtained by fitting τ values above 5.5 K based on the Arrhenius equation $\tau = \tau_0 \exp(-\Delta E/k_B T)$, giving the pre-exponential factor $\tau_0 = 1.05\times10^{-8}$ s and the energy barrier $\Delta E/k_B = 50.33$ K. The result of τ_0 is consistent with the expected value of 10^{-6}–10^{-12} s and comparable to those of reported SMMs.[31]

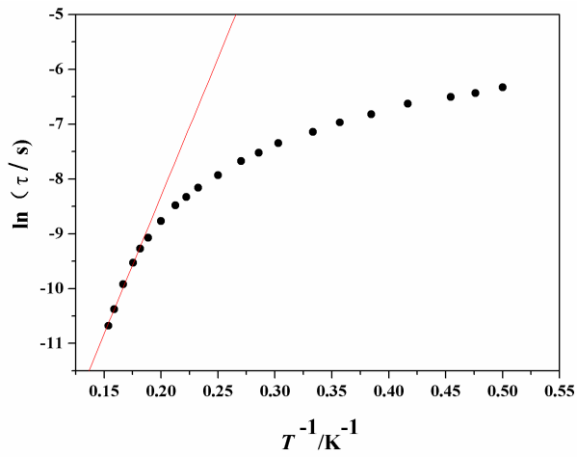

Fig. 7 Magnetization relaxation time, ln(τ) vs T^{-1} plot under H_{dc} = 0; the red line is fitted with the Arrhenius equation.

Using the frequency dependences of the ac susceptibility measurements, the Cole-Cole plots of χ'' vs χ' for **4** were obtained and fitted to the generalized Debye model to obtain the α values (Fig. S10, ESI).[32] Analysis of the cole-cole plots shows a nearly semi-circle shape and α = 0.04~0.20 over the temperature range of 3–7 K, indicating the presence of a narrow distribution of relaxation times in the dysprosium complex.

The indicative parameter of the spin disorder φ of 0.29 can be extracted based on the Mydosh formula $\varphi = (\Delta T_p/T_p)/\Delta(\log\omega)$[33] and falls into the normal range ($0.1 < \varphi < 0.3$)[32, 33] expected for a super-paramagnet, which suggested the magnetic behavior of complex **4** could not originate spin glass behavior.

For lanthanide-based complexes, slow magnetic relaxation is often attributed to single-ion behavior due to weak exchange interactions between lanthanide ions, in which the strength and symmetry of the local crystal field around the lanthanide ion plays a critical role. The material $Dy(hfac)_3{\cdot}2H_2O$ has been confirmed to show practically no SMM behavior, [34] while complex **4** shows the typical features associated with SMM behavior. This result may be due to the high symmetry environments around the Dy^{III} in $Dy(hfac)_3{\cdot}2H_2O$, while the distorted coordination environment around Dy^{III} has lower symmetry in complex **4** due to the hfac and, especially, the 2-(2′-benzothiazole)-8-hydroxyquinoline ligand, which lifts the 16-fold

degeneracy of the J = 15/2 ground multiplet of Dy^{III} ions. The lowest doubly degenerate sublevels that formally correspond to large $J_z = \pm 15/2$[35] or $J_z = \pm 13/2$[36] for dysprosium are considerably separated from the remainder of the sub-states,[37] resulting in strong uniaxial magnetic anisotropy and a higher thermal barrier.

Conclusions

In summary, seven new lanthanide complexes were synthesized using 2-(2′-benzothiazole)-8-hydroxyquinoline and hexafluoroacetylacetonate as ligands. These compounds are μ-phenol bridged dinuclear complexes. Complexes **1** and **3** show the characteristic peaks of lanthanide ions. In addition, a broad emission band resulting from ligand fluorescence is also detected, which indicates that efficiency of the energy transfer from the ligands to the ions is not ideal due to the mismatch of the energy level between L ligands and the lanthanide ions. Meanwhile, complex **4** and **7** exhibits ligand-centered fluorescence at room temperature. The magnetic study reveals that **2** displays a magnetocaloric effect. Dynamic magnetic studies reveal that complex **4** exhibits slow magnetic relaxation in the absence of an applied dc field, which is one of the main characteristics of single-molecule magnets (SMMs). Compared with $Dy(hfac)_3 \cdot 2H_2O$, complex **4** exhibits SMM behavior possibly due to the distorted coordination environment around Dy^{III}, which has lower symmetry, due to the hfac and 2-(2′-benzothiazole)-8-hydroxyquinoline ligands.

Experimental section

Materials and general methods.

All chemicals and solvents were commercially available and used without further purification. Elemental analyses for C, H and N were performed on a PerkinElmer 240 CHN elemental analyzer. IR spectra were recorded in the range of 400−4000 cm^{-1} with a Bruker TENOR 27 spectrophotometer using a KBr pellet. Thermogravimetric analysis (TGA)

experiments were obtained using a NETZSCHTG 209 thermal analyzer in a static atmosphere with a sample size and a heating rate of 10 °C min^{-1}. Powder X-ray diffraction (PXRD) measurements were collected on a Rigaku D/max 2500/pc/X-ray powder diffractometer with Cu-*Kα* radiation (*λ* = 1.540598 Å). UV–vis spectra were collected on a TU-1901 spectrophotometer at room temperature. The fluorescent spectra were measured on a Varian Cary Eclipse Fluorescence spectrophotometer at room temperature. NIR spectra were measured on a Horiba Jobin Yvon Fluorolog-3-tau fluorescence spectrophotometer, equipped with a 450 W Xe-lamp as the excitation source and a liquid-nitrogen-cooled InGaAs as detector. Magnetic measurements were performed using an MPMS XL-7 SQUID magnetometer. ^{1}H NMR spectra were obtained using a 400 MHz NMR spectrometer.

Preparation of dinuclear lanthanide complexes [$Ln_2(hfac)_4L_2$] (Ln = Eu (1), Gd (2), Tb (3), Dy (4), Ho (5), Er (6), Lu (7)). All seven of the complexes were synthesized by the same method. $Ln(hfac)_3{\cdot}2H_2O$ (0.025 mmol) was dissolved in 20 mL of acetonitrile and then heated to 70 °C. A 5 mL CH_2Cl_2 solution of HL (0.025 mmol) was added. The mixture was heated for 1 h at approximately 70 °C and then cooled to room temperature. After being filtered, the filtrate was concentrated by slow evaporation at 4 °C. After a few days, yellow crystals suitable for single-crystal X-ray analysis were obtained.

[$Eu_2(hfac)_4L_2$] (**1**). Yield: 0.0211 g, 50% based on Eu. Anal. Calcd (%) for $C_{52}H_{22}F_{24}Eu_2N_4O_{10}S_2$ (fw = 1686.78): C, 37.03; H, 1.32; N, 3.32; Found: C, 36.99; H, 1.29; N, 3.27%. IR (cm^{-1}): 1651s, 1487m, 1460m, 1379w, 1320w, 1253s, 1216m, 1195m, 1143s, 1098m, 835w, 799w, 758w, 658w.

[$Gd_2(hfac)_4L_2$] (**2**). Yield: 0.0221 g, 52% based on Gd. Anal. Calcd (%) for $C_{52}H_{22}F_{24}Gd_2N_4O_{10}S_2$ (fw = 1697.36): C, 36.80; H, 1.31; N, 3.30; Found: C, 36.78; H, 1.28; N, 3.27%. IR (cm^{-1}): 1652s, 1487m, 1460m, 1378w, 1320w, 1253s, 1215m, 1195m, 1143s, 1098m, 835w, 798w, 758w, 658w.

[**$Tb_2(hfac)_4L_2$**] (**3**). Yield: 0.0234 g, 55% based on Tb. Anal. Calcd (%) for $C_{52}H_{22}F_{24}Tb_2N_4O_{10}S_2$ (fw = 1700.70): C, 36.73; H, 1.30; N, 3.29; Found: C, 36.69; H, 1.28; N, 3.26%. IR (cm^{-1}): 1652s, 1484m, 1460m, 1377w, 1322w, 1253s, 1216m, 1196m, 1143s, 1098m, 834w, 799w, 758w, 658w.

[**$Dy_2(hfac)_4L_2$**] (**4**). Yield: 0.0209 g, 49% based on Dy. Anal. Calcd (%) for $C_{52}H_{22}F_{24}Dy_2N_4O_{10}S_2$ (fw = 1707.86): C, 36.57; H, 1.30; N, 3.28; Found: C, 36.54; H, 1.27; N, 3.25%. IR (cm^{-1}): 1652s, 1486m, 1458m, 1378w, 1321w, 1252s, 1216m, 1195m, 1142s, 1097m, 833w, 799w, 760w, 658w.

[**$Ho_2(hfac)_4L_2$**] (**5**). Yield: 0.0231 g, 54% based on Ho. Anal. Calcd (%) for $C_{52}H_{22}F_{24}Ho_2N_4O_{10}S_2$ (fw = 1712.72): C, 36.47; H, 1.29; N, 3.27; Found: C, 36.45; H, 1.25; N, 3.24%. IR (cm^{-1}): 1653s, 1487m, 1461m, 1377w, 1320w, 1253s, 1214m, 1196m, 1144s, 1100m, 835w, 799w, 758w, 658w.

[**$Er_2(hfac)_4L_2$**] (**6**). Yield: 0.0241 g, 56% based on Er. Anal. Calcd (%) for $C_{52}H_{22}F_{24}Er_2N_4O_{10}S_2$ (fw = 1717.38): C, 36.37; H, 1.29; N, 3.26; Found: C, 36.36; H, 1.27; N, 3.24%. IR (cm^{-1}): 1654s, 1488m, 1461m, 1377w, 1320w, 1253s, 1216m, 1195m, 1144s, 1100m, 835w, 799w, 758w, 659w.

[$Lu_2(hfac)_4L_2$] (**7**). Yield: 0.0247 g, 57% based on Lu. Anal. Calcd (%) for $C_{52}H_{22}F_{24}Lu_2N_4O_{10}S_2$ (fw = 1732.80): C, 36.05; H, 1.28; N, 3.23; Found: C, 36.08; H, 1.27; N, 3.20%. IR (cm^{-1}): 1652s, 1487m, 1460m, 1378w, 1320w, 1253s, 1215m, 1195m, 1143s, 1098m, 835w, 798w, 758w, 658w.

Single-crystal X-ray structure determination.

The single-crystal X-ray diffraction data for complexes **1**–**7** were collected using a BRUKER SMART-1000 CCD diffractometer equipped with graphite-monochromatized Mo-Kα radiation with a radiation wavelength of 0.071073 nm using the ω-φ scan technique. The structures were solved by direct methods using the program SHELXS-97,[38] and refined

anisotropically using the full-matrix least-squares technique based on F^2 using SHELXL-97.[38] Anisotropic thermal parameters were assigned to all non-hydrogen atoms. The hydrogen atoms were generated geometrically. Crystal data collection and refinement details for complexes **1**–**7** are summarized in Table 1.

Table 1 Crystal data and structure refinement for complexes 1–**7**

Complex	**1**	**2**	**3**	**4**	**5**	**6**	**7**
Formula	$C_{52}H_{22}F_{24}Eu_2N_4O_{10}S_2$	$C_{52}H_{22}F_{24}Gd_2N_4O_{10}S_2$	$C_{52}H_{22}F_{24}Tb_2N_4O_{10}S_2$	$C_{52}H_{22}F_{24}Dy_2N_4O_{10}S_2$	$C_{52}H_{22}F_{24}Ho_2N_4O_{10}S_2$	$C_{52}H_{22}F_{24}Er_2N_4O_{10}S_2$	$C_{52}H_{22}F_{24}Lu_2N_4O_{10}S_2$
Formula weight	1686.78	1697.36	1700.70	1707.86	1712.72	1717.38	1732.80
Temperature (K)	113(2)	113(2)	113(2)	113(2)	113(2)	113(2)	113(2)
Wavelength (Å)	0.71073	0.71073	0.71073	0.71073	0.71073	0.71073	0.71073
Crystal system	Monoclinic	Monoclinic	Monoclinic	Monoclinic	Monoclinic	Monoclinic	Monoclinic
Space group	*C2/c*	*C2/c*	*C2/c*	*C2/c*	*C2/c*	*C2/c*	*C2/c*
a (Å)	23.754(5)	23.689(5)	23.548(5)	23.555(5)	23.527(5)	23.436(5)	23.323(5)
b (Å)	12.591(3)	12.600(3)	12.604(3)	12.633(3)	12.638(3)	12.644(3)	12.666(3)
c (Å)	20.266(4)	20.254(4)	20.197(4)	20.210(4)	20.219(4)	20.176(4)	20.143(4)
α (deg)	90	90	90	90	90	90	90
β (deg)	104.94(3)	105.14(3)	104.93(3)	105.17(3)	105.16(3)	105.12(3)	105.32(3)
γ (deg)	90	90	90	90	90	90	90
Volume ($Å^3$)	5856(2)	5836(2)	5792(2)	5804(2)	5803(2)	5772(2)	5739(2)
Z	4	4	4	4	4	4	4
Calculated density (Mg m^{-3})	1.913	1.932	1.950	1.954	1.961	1.976	2.006
Absorption coefficient (mm^{-1})	2.330	2.462	2.632	2.764	2.917	3.099	3.632
F (000)	3264	3272	3280	3288	3296	3304	3328
θ range for data collection (deg)	1.84 to 27.90	1.78 to 27.88	1.79 to 27.92	1.79 to 27.91	1.79 to 27.89	1.80 to 27.90	1.81 to 27.94
Reflections collected	28301	28815	28491	22000	28632	28305	28997
Independent reflection	6985 [R(int) = 0.0301]	6975 [R(int) = 0.0304]	6940[R(int) =0.0324]	6880[R(int)=0.0349]	6933[R(int)=0.0375]	6848[R(int)=0.0354]	6849 [R(int) = 0.0466]
Completeness	99.6%	99.9%	99.7%	98.8%	99.7%	98.9%	99.2%
Max. and min. transmission	0.7674 and 0.6529	0.7566 and 0.6388	0.7430 and 0.6211	0.7326 and 0.6078	0.7210 and 0.5931	0.7074 and 0.5761	0.6697 and 0.5303
Data / restraints / parameters	6985 / 120 / 444	6975 / 153 / 481	6940 / 402 / 480	6880 / 153 / 484	6933 / 84 / 474	6848 / 153 / 478	6849 / 120 / 480
Goodness-of-fit on F^2	1.050	1.038	1.169	1.068	1.171	1.117	1.116
Final R indices [$I>2\sigma(I)$]	R_1 = 0.0297, wR_2 = 0.0719	R_1 = 0.0289, wR_2 = 0.0748	R_1 = 0.0326, wR_2 = 0.0738	R_1 = 0.0346, wR_2 = 0.0743	R_1 = 0.0298, wR_2 = 0.0722	R_1 = 0.0265, wR_2 = 0.0661	R_1 = 0.0286, wR_2 = 0.0750
R indices (all data)	R_1 = 0.0333, wR_2 = 0.0738	R_1 = 0.0339, wR_2 = 0.0805	R_1 = 0.0373, wR_2 = 0.0763	R_1 = 0.0433, wR_2 = 0.0787	R_1 = 0.0352, wR_2 = 0.0782	R_1 = 0.0309, wR_2 = 0.0682	R_1 = 0.0337, wR_2 = 0.0771
Largest diff. peak and hole(e $Å^{-3}$)	1.455 and -1.332	1.438 and -0.905	1.305 and -1.318	1.268 and -1.360	0.855 and -1.803	0.883 and -1.323	1.041 and -1.977

Acknowledgments

This work was financially supported by the National Natural Science Foundation of China (Nos. 21473121, 21271137).

References

1 (*a*) M. C. Heffern, L. M. Matosziuk and T. J. Meade, *Chem. Rev.*, 2014, **114**, 4496; (*b*) S. V. Eliseeva and J. C. G. Bunzli, Chem. *Soc. Rev.*, 2010, **39**, 189.

2 (*a*) X. Ma, X. Li, Y.-E. Cha and L.-P. Jin, *Cryst. Growth Des.*, 2012, **12**, 5227; (*b*) B. Xu, Q. Chen, H.-M. Hu, R. An, X.-F. Wang and G.-L. Xue, *Cryst. Growth Des.*, 2015, **15**, 2318.

3 (*a*) J. Bunzli, *Chem. Rev.*, 2010, **110**, 2729; (*b*) Y. Cui, Y. Yue, G. Qian and B. Chen, *Chem. Rev.*, 2012, **112**, 1126; (*c*) J. F. Lemonnier, L. Guenee, C. Beuchat, T. A. Wesolowski, P. Mukherjee, D. H. Waldeck, K. A. Gogick, S. Petoud and C. Piguet, *J. Am. Chem. Soc.*, 2011, **133**, 16219.

4 (*a*) H.-S. Peng, M. I. J. Stich, J.-B. Yu, L.-N. Sun, L. H. Fischer and O. S. Wolfbeis, *Adv. Mater.*, 2010, **22**, 716; (*b*) L.-N. Sun, X.-Q. Ge, J.-L. Liu, Y.-N. Qiu, Z.-W. Wei, B. Tian and L.-Y. Shi, *Nanoscale*, 2014, **6**, 13242.

5 (*a*) N. Domingo, E. Bellido and D. Ruiz-Molina, *Chem. Soc. Rev.*, 2012, **41**, 258; (*b*) S. Sanvito, *Chem. Soc. Rev.*, 2011, **40**, 3336.

6 F. Troiani and M. Affronte, *Chem. Soc. Rev.*, 2011, **40**, 3119.

7 (*a*) J. Camarero and E. Coronado, *J. Mater. Chem.*, 2009, **19**, 1678; (*b*) Y.-Z. Zheng, G.-J. Zhou, Z.-P. Zheng and R. E. P. Winpenny, *Chem. Soc. Rev.*, 2014, **43**, 1462.

8 (*a*) Y. Meng, Y.-C. Chen, Z.-M. Zhang, Z.-J. Lin and M.-L. Tong, *Inorg. Chem.*, 2014, **53**, 9052; (*b*) J. W. Sharples, Y.-Z. Zheng, F. Tuna, E. J. L. McInnes and D. Collison, *Chem. Commun.*, 2011, **47**, 7650.

9 M. Mannini, F. Pineider, C. Danieli, F. Totti, L. Sorace, P. Sainctavit, M. A. Arrio, E. Otero, L. Joly, J. C. Cezar, A. Cornia and R. Sessoli, *Nature*, 2010, **468**, 417.

10 W. Wernsdorfer and R. Sessoli, *Science*, 1999, **284**, 133.

11 L. Lecren, W. Wernsdorfer, Y.-G. Li, O. Roubeau, H. Miyasaka and R.Clérac, *J. Am. Chem. Soc.*, 2005, **127**, 11311.

12 S. Hill, R. S. Edwards, N.Aliaga-Alcalde and G. Christou, *Science*, 2003, **302**, 1015.

13 (*a*) F. Habib and M. Murugesu, *Chem. Soc. Rev.*, 2013, **4**2, 3278; (*b*) F. Tuna, C. A. Smith, M. Bodensteiner, L. Ungur, L. F. Chibotaru, E. J. L. McInnes, R. E. P. Winpenny, D. Collison and R. A. Layfield, *Angew. Chem. Int. Ed.*, 2012, **51**, 6976; (*c*) L. Ungur, S.-Y. Lin, J.-K. Tang and L. F. Chibotaru, *Chem. Soc. Rev.*,

2014, **43**, 6894; (*d*) N. M. Randell, M. U. Anwar, M. W. Drover, L. N. Dawe and L. K. Thompson, *Inorg. Chem.*, 2013, **52**, 6731; (*e*) R. J. Blagg, C. A. Muryn, E. J. L. McInnes, F. Tuna and R. E. P. Winpenny, *Angew. Chem. Int. Ed.*, 2011, **50**, 6530; (*f*) Y.-L. Hou, G. Xiong, P.-F. Shi, R.-R. Cheng, J.-Z. Cui and B. Zhao, *Chem. Commun.*, 2013, **49**, 6066; (*g*) B. Joarder, S. Mukherjee, S. Xue, J. Tang and S. K. Ghosh, *Inorg. Chem.*, 2014, **53**, 7554.

14 (*a*) L.-X. Chang, G. Xiong, L. Wang, P. Cheng and B. Zhao, *Chem. Commun.*, 2013, **49**, 1055; (*b*) S. Biswas, A. Adhikary, S. Goswami and S. Konar, *Dalton Trans.*, 2013, **42**, 13331; (*c*) Y. Yang, Q.-C. Zhang, Y.-Y. Pan, L.-S. Long and L.-S. Zheng, *Chem. Commun.*, 2015, **51**, 7317; (*d*) A. Adhikary, J. A. Sheikh, S. Biswas and S. Konar, *Dalton Trans.*, 2014, **43**, 9334; (*e*) J.-B. Peng, X.-J. Kong, Q.-C. Zhang, M. Orendáč, J. Prokleška, Y.-P. Ren, L.-S. Long, Z. Zheng and L.-S. Zheng, *J. Am. Chem. Soc.*, 2014, **136** (52), 17938; (*f*) S. Biswas, H. S. Jena, A. Adhikary and S. Konar, *Inorg. Chem.*, 2014, **53**, 3926; (*g*) O. Roubeau, G. Lorusso, S. J. Teat and M. Evangelisti, *Dalton Trans.*, 2014, **43**, 11502; (*h*) S.-J. Liu, J.-P. Zhao, J. Tao, J.-M. Jia, S.-D. Han, Y. Li, Y.-C. Chen and X.-H. Bu, *Inorg. Chem.*, 2013, **52**, 9163; (*i*) S.-J. Liu, C.-C. Xie, J.-M. Jia, J.-P. Zhao, S.-D. Han, Y. Cui, Y. Li and X.-H. Bu, *Chem.–Asian J.*, 2014, **9**, 1116.

15 (*a*) V. Chandrasekhar, S. Hossain, S. Das, S. Biswas and J.-P. Sutter, *Inorg. Chem.*, 2013, **52**, 6346; (*b*) N. F. Chilton, G. B. Deacon, O. Gazukin, P. C. Junk, B. Kersting, S. K. Langley, B. Moubaraki, K. S. Murray, F. Schleife, M. Shome, D. R.Turner and J. A. Walker, *Inorg. Chem.*, 2014, **53**, 2528; (*c*) F.-Z. Duan, L.-Z. Liu, C.-Y. Qiao and H.-M. Yang, *Inorg. Chem. Commun.*, 2015, **55**, 120.

16 S.-J. Li, *Luminescence*, 2012, **27**, 242.

17 (*a*) N. M. Shavaleev, R. Scopelliti, F. Gumy and J.-C. G. Bünzli, *Inorg. Chem.*, 2009, **48**, 2908; (*b*) N. M. Shavaleev, R. Scopelliti, F. Gumy and J.-C. G. Bünzli, Inorg. Chem., 2009, **48**, 7937; (*c*) N. M. Shavaleev, R. Scopelliti, F. Gumy and J.-C. G. Bünzli, *Inorg. Chem.*, 2008, **47**, 9055.

18 J.-Q. Zhang, H.-F. Li, P. Chen, W.-B. Sun, T. Gao and P.-F. Yan, *J. Mater. Chem. C*, 2015, **3**, 1799.

19 G. A. Crosby, R. M. Alire and R. E. Whan, *J. Chem. Phys.*, 1961, **34**, 743.

20 M. Latva, H. Takalo, V. M. Mukkala, C. Matachescu, J. C. Rodriguez-Ubis and J. Kankare, *J. Lumin.*, 1997, **75**, 149.

21 H.-B. Xu, J. Li, L.-X. Shi and Z.-N. Chen, *Dalton Trans.*, 2011, **40**, 5549.

22 Y.-L. Wang, Y. Ma, X. Yang, J.-K. Tang, P. Cheng, Q.-L. Wang, L.-C. Li and D.-Z. Liao, *Inorg. Chem.*, 2013, **52**, 7380.

23 (*a*) R.-H. Wang, L. Han, F.-L. Jiang, Y.-F. Zhou, D.-Q. Yuan and M.-C. Hong, Cryst. *Growth Des.*, 2005, **5**, 129; (*b*) L.-L. Wen, D.-B. Dang, C.-Y. Duan, Y.-Z. Li, Z.-F. Tian and Q.-J. Meng, *Inorg. Chem.*, 2005, **44**, 7161; (*c*) W.-T. Xu, Y.-F. Zhou, D.-C. Huang, W. Xiong, M.-Y. Su, K. Wang, S. Han and M.-C. Hong, *Cryst. Growth Des.*, 2013, **13**, 5420.

24 (*a*) L.-N. Sun, Y.-N. Qiu, T. Liu, J.-Z. Zhang, S. Dang, J. Feng, Z.-J. Wang, H.-J. Zhang and L.-Y. Shi, *ACS Appl. Mater. Interfaces*, 2013, 5, 9585; (*b*) L.-N. Sun, S. Dang, J.-B. Yu, J. Feng, L.-Y. Shi and H.-J. Zhang, *J. Phys. Chem. B*, 2010, **114**, 16393.

25 Z. Ahmed and K. Iftikhar, *J. Phys. Chem. A*, 2013, **117**, 11183.

26 D. Aguilà, L. A. Barrios, V. Velasco, L. Arnedo, N. Aliaga-Alcalde, M. Menelaou, S. J. Teat, O. Roubeau, F. Luis and G. Aromí, *Chem.–Eur. J.*, 2013, **19**, 5881.

27 W.-T. Xu, Y.-F. Zhou, D.-C. Huang, W. Xiong, M.-Y. Su, K. Wang, S. Han and M.-C. Hong, *Cryst. Growth Des.*, 2013, **13**, 5420.

28 (*a*) G. Lorusso, M. A. Palacios, G. S. Nichol, E. K. Brechin, O. Roubeau and M. Evangelisti, *Chem. Commun.*, 2012, **48**, 7592; (*b*) Y. Li, J.-W. Yu, Z.-Y. Liu, E.-C. Yang and X.-J. Zhao, *Inorg. Chem.*, 2015, **54**, 153; (*c*) S.-D. Han, X.-H. Miao, S.-J. Liu and X.-H. Bu, *Inorg. Chem. Front.*, 2014, **1**, 549; (*d*) J.-M. Jia, S.-J. Liu, Y. Cui, S.-D. Han, T.-L. Hu and X.-H. Bu, *Cryst. Growth Des.*, 2013, **13**, 4631.

29 Y.-C. Chen, F.-S. Guo, Y.-Z. Zheng, J.-L. Liu, J.-D. Leng, R. Tarasenko, M. Orendáč, J. Prokleška, V. Sechovský and M.-L. Tong, *Chem.−Eur. J.*, 2013, **19**, 13504.

30 S. Osa, T. Kido, N. Matsumoto, N. Re, A. Pochaba and J. Mrozinski, *J. Am. Chem. Soc.*, 2004, **126**, 420.

31 (*a*) P. Zhang, L. Zhang and J.-K. Tang, *Dalton Trans.*, 2015, **44**, 3923; (*b*) K. Suzuki, R. Sato and N. Mizuno, *Chem. Sci.*, 2013, **4**, 596; (*c*) P. Bag, C. K. Rastogi, S. Biswas, S. Sivakumar, V. Mereacre and V. Chandrasekhar, *Dalton Trans.*, 2015, **44**, 4328.

32 J. A. Mydosh, *Spin Glasses: An Experimental Introduction*, Taylor & Francis, London, 1993.

33 N. Ishii, Y. Okamura, S. Chiba, T. Nogami and T. Ishida, *J. Am. Chem. Soc.*, 2008, **130**, 24.

34 F. Mori, T. Nyui, T. Ishida, T. Nogami, K. Y. Choi and H. Nojiri, *J. Am. Chem. Soc.*, 2006, **128**, 1440.

35 T. Yamaguchi, Y. Sunatsuki, H. Ishida, M. Kojima, H. Akashi, N. Re, N. Matsumoto, A Pochaba and J. Mroziński. *Inorg. Chem.*, 2008, **47**, 5736.

36 (*a*) S. Takamatsu and N. Ishikawa, *Polyhedron*, 2007, **26**, 1859; (*b*) N. Ishikawa, *Polyhedron*, 2007, **26**, 2147.

37 F. Pointillart, K. Bernot, R. Sessoli and D. Gatteschi, *Chem.–Eur. J.*, 2007, **13**, 1602.

38 G. M. Sheldrick, *SHELXS-97*, Program for the Solution of Crystal Structures; University of Göttingen: Göttingen, Germany, 1997.